Slick (Kcnt2) Sodium-Activated Potassium Channels Limit Peptidergic Nociceptor Excitability and Hyperalgesia

Journal of Experimental Neuroscience
Volume 11: 1–16

DOI: 10.1177/1179069517726996

Danielle L Tomasello[1], Edward Hurley[2], Lawrence Wrabetz[2] and Arin Bhattacharjee[1,3]

[1]Neuroscience Program, The State University of New York – University at Buffalo, Buffalo, NY, USA. [2]Department of Neurology, Jacobs School of Medicine and Biomedical Sciences, The State University of New York – University at Buffalo, Buffalo, NY, USA. [3]Department of Pharmacology and Toxicology, Jacobs School of Medicine and Biomedical Sciences, The State University of New York – University at Buffalo, Buffalo, NY, USA.

ABSTRACT: The Slick (Kcnt2) sodium-activated potassium (K_{Na}) channel is a rapidly gating and weakly voltage-dependent and sodium-dependent potassium channel with no clearly defined physiological function. Within the dorsal root ganglia (DRGs), we show Slick channels are exclusively expressed in small-sized and medium-sized calcitonin gene–related peptide (CGRP)-containing DRG neurons, and a pool of channels are localized to large dense-core vesicles (LDCV)-containing CGRP. We stimulated DRG neurons for CGRP release and found Slick channels contained within CGRP-positive LDCV translocated to the neuronal membrane. Behavioral studies in Slick knockout (KO) mice indicated increased basal heat detection and exacerbated thermal hyperalgesia compared with wild-type littermate controls during neuropathic and chronic inflammatory pain. Electrophysiologic recordings of DRG neurons from Slick KO mice revealed that Slick channels contribute to outward current, propensity to fire action potentials (APs), and to AP properties. Our data suggest that Slick channels restrain the excitability of CGRP-containing neurons, diminishing pain behavior after inflammation and injury.

KEYWORDS: Ion channels, CGRP, chronic pain, DRG neurons, thermal nociception

RECEIVED: April 19, 2017. **ACCEPTED:** July 25, 2017.

PEER REVIEW: Two peer reviewers contributed to the peer review report. Reviewers' reports totaled 1095 words, excluding any confidential comments to the academic editor.

TYPE: Original Research

FUNDING: The author(s) disclosed receipt of the following financial support for the research, authorship, and/or publication of this article: This work was supported by National Institutes of Health Grant NS078184 (to A.B.).

DECLARATION OF CONFLICTING INTERESTS: The author(s) declared no potential conflicts of interest with respect to the research, authorship, and/or publication of this article.

CORRESPONDING AUTHOR: Arin Bhattacharjee, Department of Pharmacology and Toxicology, Jacobs School of Medicine and Biomedical Sciences, The State University of New York – University at Buffalo, 102 Farber Hall, 3435 Main Street, Buffalo, NY 14214, USA. Email: ab68@buffalo.edu

Through the study of basic mechanisms in pain transmission, many molecules that promote nociception have been identified, including sodium channels Navs1.7-9, the capsaicin-sensitive Transient Receptor Potential Vanilloid 1 (TRPV1) channel, purinergic receptors, acid-sensing ion channels, and recently the calcium-activated chloride channel Ano1.[1] Included in this expansive list are neuroinflammatory peptides substance P (SP) and calcitonin gene–related peptide (CGRP). Calcitonin gene–related peptide is contained within a subset of nociceptive, small-sized and medium-sized neurons in the trigeminal ganglia (TG) and dorsal root ganglia (DRGs).[2] It could be argued that because molecules that promote nociception are so effective in their ability to transduce pain signals, there needs to be a counterbalance to these molecules and pathways to moderate their effects.

Potassium channels specifically expressed in pain-sensing DRG neurons can diminish nociception because of their inherent abilities to reduce neuronal excitability.[3] One family of potassium channels, called K_{Na} channels, are comprised of the Slack (Kcnt1, Slo2.2, KNa1.1) and Slick (Kcnt2, Slo2.1, KNa1.2) subunits. These channels are thought to reduce excitability.[4] Both Slack and Slick channels have large unitary conductance and are activated by sodium, but the channels exhibit distinct activation kinetics on step depolarizations.[5] Specific roles for Slack channels in DRG neuronal firing and pain have been identified. These channels are ubiquitously expressed in rat DRG neurons,[6] and protein kinase A–dependent internalization of Slack channels from the DRG neuronal membrane was shown to be associated with a loss of firing accommodation resembling nociceptor sensitization.[7] Furthermore, studies from Slack knockout (KO) mice and rats treated with Slack-specific small interfering RNAs indicated enhanced itch and pain responses along with heightened mechanical allodynia during neuropathic pain.[8–10] There is yet to be a physiological role credited to Slick K_{Na} channels.

In comparison with the canonical sequence of Slack,[11] the Slick channel amino acid sequence is highly homologous with a notable difference in its amino terminal.[12] However, there is significant divergence in channel properties. Namely, Slick channels have rapid gating kinetics, higher reactivity to intracellular chloride, decreased sensitivity to intracellular sodium, basal level of activity in the absence of sodium, weak voltage dependence,[13] and increased sensitivity to small changes in cell volume.[14] Computer simulations proposed that the instantaneous activation properties of Slick channels might affect the elicitation of an action potential (AP) and during sustained depolarizations to reduce the number of APs fired.[15] Taken together, these unique biophysical

properties would predict that Slick channels have a very specific role in regulating neuronal excitability.

We sought to determine the physiological role of Slick channels in DRG neurons and how the channels affect the processing of pain. Here, we report that Slick channels within DRG and TG are exclusively expressed in CGRP-containing neurons, and a pool of channels colocalize to large dense-core vesicles (LDCV)-containing CGRP. Using a previously uncharacterized global Slick-LacZ KO mouse line, we determined that KO mice exhibit a thermal hyperalgesic phenotype and Slick channels shape AP properties. This study identifies a physiological function for Slick channels in moderating nociception.

Methods

Slick KO mice

Kcnt2 KO mice, background strain C57Bl6/J/129 mixed, were a generous gift from Sanofi R&D, France. All experiments were performed on littermates. The transgene consisted of the replacement of exons 2 to 7, encoding the transmembrane domains and pore of *Slick Kcnt2* channel gene, with a LacZ LoxP-UB1 EM7 Neo-LoxP cassette. The LacZ exon with a stop codon becomes fused to the exon encoding for amino acid 33, and the resultant insertion created a frameshift in the remaining transcript after stop codon. The total deletion size within gene was 25,218 nucleotides.

Immunohistochemistry

Mice were anesthetized with a high dose of sodium pentobarbital and perfused transcardially with 4% paraformaldehyde (PFA). Lumbar DRGs, lumbar spinal cord, sciatic nerve connected to lumbar DRGs, and paws were removed from the fixed mice and postfixed overnight. Tissue was then cryoprotected in phosphate-buffered saline (PBS) containing 30% sucrose overnight. After embedding in freezing media, tissue was sliced on cryostat at a size of 15 µm. Slices were permeabilized with a PBS solution containing 0.2% Triton X-100. Sections were then blocked for 2 hours at room temperature with PBS containing 3% bovine serum albumin (BSA). Sections were then incubated with a mixture of primary antibodies in PBS containing 3% BSA overnight at 4°C. Primary antibodies included Slick anti-mouse (1:250; NeuroMab, Davis, CA, USA), CGRP anti-goat (1:2000; Abcam), Substance-P anti-guinea pig (1:2000; Abcam, Cambridge, MA, USA), and Slack anti-chicken (1:750; Bhattacharjee et al[5]). The Slick NeuroMab antibody has been successfully used for immunohistochemistry (IHC) studies.[16,17] After several rinses, secondary antibodies including Alexa Fluor 633 anti-mouse, Alexa Fluor 488 anti-goat, Alexa Fluor 546 anti-chicken, and Alexa Fluor 546 anti-guinea pig were added (1:1000) to PBS containing 3% BSA for 2 hours (Life Technologies, Thermo Fisher Scientific, Waltham,MA, USA). Tissue was then mounted on slides using ProLong Gold Antifade Reagent with 4,6-diamidino-2-phenylindole dihydrochloride (DAPI; Life Technologies).

All imaging was performed on a Zeiss AxioImager Z1 Axiophot wide-field fluorescence, with Apotome for optical sectioning. Optimal antibody concentration and exposure time, for each antibody and tissue type, was determined at initial tissue imaging. The same exposure time was used for each tissue type. After exposure, min/max range was selected for optimal contrast and to minimize background. Quantification of relative integrated density of immunofluorescence of individually isolated lumbar DRG soma was done by ImageJ. Raw exported images were opened in ImageJ, followed by freehand isolation of individual DRGs determined by the presence of DAPI. Measurements were taken for each fluorescent channel, where then integrated density was used for quantitative analysis. All tissue was processed under identical fixation and developmental conditions. For 3,3′-diaminobenzidine (DAB)-enhanced sciatic nerve staining, Slick anti-chicken (Bhattacharjee et al[15]) was used as primary antibody. The next day, a Vectastain Elite ABC Mouse IgG Kit (Vector Labs, Burlingame, CA, USA) was used for primary antibody detection using a 1:750 dilution of biotinylated chicken secondary antibody. The DAB reaction was applied for 15 minutes. Each experiment was performed in at least 3 animals per condition specified.

LDCV fractionation

The protocol was adapted from Zhao et al.[18] Briefly, adult mouse DRGs were collected (about 40 DRGs), then homogenized and centrifuged to isolate cells. The resulting pellet was resuspended in osmotic lysis buffer to lyse synaptosomes and then centrifuged. Next, the pellet was resuspended in sucrose buffer and layered onto a continuous sucrose gradient. In the first centrifugation step, the sucrose gradient ranged from 0.3 to 1.2 M sucrose. Samples were collected, and equal-volume aliquots were analyzed by immunoblotting Chromogranin-B anti-mouse (1:1000; Santa Cruz Biotechnology Inc., Santa Cruz, CA, USA). The LDCV fractions with Chr-B positive bands were diluted with 0.3 M sucrose and centrifuged. The pellet was resuspended in sucrose buffer, layered onto the second sucrose gradient from 1.1 to 2.0 M sucrose, and centrifuged. Chr-B–positive fractions were pooled and dialyzed by Slide-A-Lyzer Dialysis Cassette (Thermo Fisher Scientific, Waltham, MA, USA) and then concentrated with 30K molecular weight cutoff (Pierce Protein Biology,Thermo Fisher Scientific,Waltham, MA, USA). Samples were loaded onto any kD TGX Gel (Bio-Rad, Hercules, CA, USA). After electrophoresis, the gel was then transferred onto a nitrocellulose membrane and blocked in 5% nonfat dry milk as a blocking agent for 1 hour. Chromogranin-B anti-mouse (1:1000; Santa Cruz), Slick anti-mouse (1:1000; NeuroMab), and Slack anti-mouse (1:1000; NeuroMab) antibodies were used for final LDCV-positive fraction Western analysis. The signal was detected using Luminata Forte HRP Substrate (EMD

Millipore, Billerica, MA, USA). Densitometric analyses of Western blots were performed with Bio-Rad GS-700 flatbed scanning densitometry.

Electron microscopy

Wild-type adult mice underwent cardiac perfusion with 4% PFA in PBS. Lumbar DRGs were excised and postfixed overnight in 4% PFA. Tissue was then placed in 30% sucrose in PBS overnight. Dorsal root ganglia were embedded in agarose and sliced on a vibratome at 40 µm. Tissue was blocked for 1 hour with 3% BSA + 0.2% Triton-X in PBS. Slick anti-mouse antibody (1:500; NeuroMab) or no antibody control was applied overnight in same solution. The next day, a Vectastain Elite ABC Mouse IgG Kit (Vector Labs) was used, with a 1:750 dilution of biotinylated mouse secondary. The DAB reaction was allowed to proceed for 2.5 minutes in the presence of primary antibody and up to 5 minutes in the absence of secondary antibody. Sections were washed with PBS and fixed with 2% glutaraldehyde overnight, then postfixed with 1% osmium tetroxide. Tissue was dehydrated in graded ethanol and embedded in Epon. Thin sections were collected and stained with uranyl acetate and lead citrate. Tissue was examined and photographed with an FEI Tecnai G2 Spirit BioTWIN electron microscope equipped with an Advanced Microscopy Techniques (AMT) 16 MegaByte mid-mount CCD camera. Experiment was repeated twice.

Primary DRG neuronal culture

For adult mouse DRG neuronal cultures, mice were euthanized with CO_2 and decapitated. The spine was removed and placed in a Petri dish with Hanks balanced salt solution (Corning, Manassas, VA, USA). Dorsal root ganglia were dissected and dissociated in 0.28 Wünsch units/mL Liberase Blendzyme (Roche Diagnostics Corporation, Indianapolis, IN, USA) for 1 hour at 37°C. Neurons were plated on poly-D-lysine (PDL) and laminin-coated coverslips and cultured in Neurobasal-A Medium (Invitrogen (Thermo Fisher Scientific), Waltham, MA, USA) supplemented with B-27 Supplement (Invitrogen), L-glutamine (Invitrogen), and β-nerve growth factor (NGF) (Harlan Bioproducts for Science, Indianapolis, IN, USA). Cultured neurons were stored in a humidified incubator in 5% CO_2 at 37°C.

For embryonic DRG neuronal culture, embryos (E13.5) from pregnant female mice or embryos (E15) from pregnant female Sprague Darley rats were used. Dorsal root ganglia were cultured in media containing NGF for 10 days (mouse) or 5 days (rat) based on time necessary for peptide expression (refer to Tomasello et al[19] for procedure).

Membrane protein biotinylation

Embryonic DRGs were pooled from E15 rats and plated on laminin and PDL 6-well plates, 3 pups per well. For stimulated CGRP release, rat-cultured DRG neurons were incubated in CO_2 chamber at 37°C for 20 minutes in a physiological potassium–containing solution containing (in mM) 140 NaCl, 5.4 KCl, 1 CaCl2, 1 MgCl2, 15.6 HEPES ((4-(2-hydroxyethyl)-1-piperazineethanesulfonic acid)), and 10 glucose, pH 7.4 or a high KCl solution containing (in mM) 95.4 NaCl, 50 KCl, 1 CaCl2, 1 MgCl2, 10 HEPES, and 10 glucose, pH 7.4. Then, 160 µL of 10-mm Sulfo-NHS-SS-Biotin (Thermo Scientific) was added to each well and incubated at room temperature for 45 minutes. A Cell Surface Protein Isolation Kit (Pierce) was used for biotinylation. Protease Inhibitor Cocktail (Sigma-Aldrich, St. Louis, MO, USA) was also added to the kit buffers. Protein was removed from beads by resuspending beads in a gel loading buffer containing sodium dodecyl sulfate (SDS) for 1 hour at room temperature. Samples were loaded onto any kD TGX Gel (Bio-Rad). After electrophoresis, the gel was then transferred onto a nitrocellulose membrane and incubated in 5% nonfat dry milk as a blocking agent for 1 hour. Antibodies Slick anti-chicken (1:1000; Bhattacharjee et al[15]), Slack anti-mouse (1:1000; NeuroMab), and Actin anti-rabbit (1:2000; Sigma) were used for Western analysis. *Note*: We used the Slick anti-chicken antibody in rat-cultured neurons because within the Slick anti-mouse antibody–binding epitope 564 to 624, at amino acid position 616, rSlick contains Ala, whereas mSlick contains Thr. In our experience, the Slick anti-mouse antibody was not optimal for detection of rSlick, necessitating the use of the Slick anti-chicken antibody. The signal was detected using Luminata Forte HRP Substrate (Millipore). Densitometric analyses of Western blots were performed by Bio-Rad GS-700 flatbed scanning densitometry (wells: low KCl [n = 2], high KCl [n = 3]).

Immunocytochemistry

After 5 days in culture, rat embryonic DRG neurons were washed with PBS, incubated with membrane marker concanavalin A-AlexaFluor 647 (Con A) (Invitrogen), fixed with fresh 4% PFA for 10 minutes, and then permeabilized in blocking solution that contained 1% BSA for 1 hour at 4°C. Neurons were incubated with Slick anti-mouse (1:250; NeuroMab) and CGRP anti-goat (1:1000; Abcam) antibodies overnight at 4°C overnight followed by a secondary Alexa Fluor 633 anti-mouse and 488 anti-goat (1:1000; Life Technologies) for 2 hours at room temperature. Coverslips were mounted on slides using ProLong Gold Antifade Reagent with DAPI (Life Technologies). Experiments repeated twice with imaging performed in more than 12 coverslips.

Colocalization analysis

Analysis was performed using Imaris software (Oxford Instruments, Abingdon, Oxfordshire, UK) to identify colocalization between CGRP and Con A membrane marker or Slick and Con A. We used the entire linear range to eliminate human subjectivity and bias when selecting intensity. Colocalization

was analyzed by time dependence with automatic threshold and probability calculated by Pearson coefficient. Roughly 85 DRG neurons per condition were analyzed.

Membrane isolation

Whole mouse brain membrane isolation by sucrose fractionation was followed according to Bhattacharjee et al.[5] Wild-type purebred C57/Bl6 mice were compared with Slick heterozygous (HET) and KO C57Bl6/J/129 mixed strain mice for initial characterization of Slick KO mouse line. Bradford assay was used for loading onto SDS-polyacrylamide gel electrophoresis gel (Bio-Rad), 30 µg total protein per lane. After electrophoresis, the gel was then transferred onto a nitrocellulose membrane and incubated in 5% nonfat dry milk as a blocking agent for 1 hour. Antibody Slick anti-mouse (1:1000; NeuroMab) was used for Western analysis. The signal was detected using Luminata Forte HRP Substrate (Millipore). Densitometric analyses of Western blots were performed by Bio-Rad GS-700 flatbed scanning densitometry. Experiment was repeated twice.

X-gal staining

Wild-type and Slick KO adult mice underwent cardiac perfusion with 4% PFA in PBS. Lumbar DRGs were excised and cryoprotected in 30% sucrose in PBS overnight. After embedding in freezing media, tissue was sliced on cryostat 15 µm and then sliced tissue was incubated in prewarmed X-gal working solution in 37°C humidified chamber for 24 hours. Coverslips were mounted on the slides with Permount (EMS, Hatfield, PA, USA). The X-gal working solution was 1:40 dilution of stock solution in dilution buffer. The stock solution contained 4% X-gal in *N,N*-dimethylformamide. Dilution buffer comprised 5 nM potassium ferricyanide crystalline, 5 nM potassium ferricyanide trihydrate, and 2 mM magnesium chloride in PBS. Each experiment was performed in at least 3 animals.

Behavioral assessments and pain models

Mice were bred and maintained in a 12-hour light/dark cycle with free access to food and water in Laboratory Animal Facility at the SUNY (The State University of New York) University at Buffalo. All animal procedures were approved by the SUNY University at Buffalo Institutional Animal Care and Use Committee (IACUC) and adhered to the National Institutes of Health guidelines. All mice used for behavioral experimentation were adult over the age of 10 weeks. Male and female groups were tested separately. Mice were group-housed from weaning age and littermates were used for experiments, 2 to 4 animals per cage. Naïve mice were used for all experiments, and multiple behavioral tests were not performed. If mice did not habituate throughout duration of entire experiment, they were removed from analysis. Animal weights and age were recorded throughout each experiment and may be reported upon request. Sample size estimates were based on previously published pain behavior models and chosen to achieve level of statistical confidence but low enough to minimize the number of animals as per IACUC guidelines. All behavioral experiments were performed in a blinded manner. Within each genotype and sex, mice were randomly assigned for experimental groups. The number of mice at beginning and end of experiment were the same.

For mechanical allodynia behavioral testing, we used an Ugo Basile Dynamic Plantar Von Frey Apparatus in ascending order of force (1-5 g force) to the plantar surface of hind paws. Mice were first habituated in the room for 2 days (15 minutes in the room, then 30 minutes in the chambers), followed by 3 days of baseline behavioral recording. Scorer was blinded as mice were randomly placed individually in cubicles. The mouse moved about freely on a metal mesh surface in an enclosed area. A 0.5-mm-diameter stainless-steel filament exerted an increasing force to the plantar surface. Paw withdrawal reflex was automatically recorded using 2 metrics: the latency until withdrawal, in seconds, and the force at which the paw was withdrawn, in grams. Maximum force was set to 5 g with cutoff of 15 seconds.

Thermal hyperalgesia behavioral experiments were performed blind with multiple experimental sessions of group caged male and female mice. Mice were first habituated in the room for 2 days (15 minutes in the room, then 30 minutes in the chambers), followed by 3 days of baseline behavioral recording. An Ugo Basile Plantar Hargreaves Apparatus was used for hyperalgesia assessment. Scoring was blinded as mice were randomly placed individually in Plexiglas cubicles mounted on a glass surface at room temperature (~25°C). The radiant heat stimulus was fixed at an IR infrared heat stimulus of 40 with the maximum time of exposure at 15 seconds. The latency to paw withdrawal was automatically recorded. The mean withdrawal latency for each hind paw was computed by averaging 3 to 6 measurements. Pain model procedures were administered the following week to prevent habituation. Sciatic nerve cuffing is an established model that loosely constricts the sciatic nerve with a polyethylene tube and induces an ipsilateral heat thermal hyperalgesia lasting around 3 weeks, along with a sustained ipsilateral mechanical allodynia lasting at least 2 months.[20] For the neuropathic model of pain, sciatic nerve cuffing by Yalcin et al was modified by anesthesia with isoflurane. Behavior was taken every 5 days after procedure, up to 25 days. For complete Freund's adjuvant (CFA) inflammatory model of pain, mice were anesthetized with isoflurane. 20 µL from CFA ampules (Thermo Scientific) was injected into the hind paw with a 28-gauge needle. For each CFA injection, CFA was taken from a new ampule ensuring that every mouse received CFA of identical activity. We observed loss of CFA activity when opened and stored over weeks in the refrigerator. 20 µL of sterile saline was injected as control. Behavior was taken 1, 4, 8, and 12 days after procedure. Caliper was used for edema measurement (Fisher Scientific, Hampton NH, USA).

For formalin testing, mice were habituated in the behavior room for 15 minutes, then 30 minutes in the formalin chamber before injection. 20 µL of 5% formalin (in sterile saline) was injected intradermally into the right hind paw and mice were placed back in chamber for video recording. Scoring was performed for 1 minute every 5 minutes, up to an hour and averaged by 2 blinded observers from video recordings.

Vaginal cytology

Protocol for vaginal cytology was followed from the work by Byers et al.[21]

Electrophysiology

Adult-cultured DRG electrophysiologic recordings were taken from neurons cultured up to 3 days. Embryonic-cultured DRG electrophysiologic recordings were taken on cultured day 10. For recordings, data were acquired using an Axopatch 200B (Molecular Devices, Sunnyvale, CA, USA), digitized, and filtered at 2 kHz using pCLAMP 9.2 (Molecular Devices) acquisition software. Data analysis was performed using Clampfit (Molecular Devices) and Origin 6.0 (OriginLab, Northampton, MA, USA). In voltage-clamp mode, current was recorded at a holding potential of −70 mV, with 200 ms pulses between −120 and +120 mV. A current-clamp protocol consisting of depolarizing steps in increments of 20 pA from −20 to 400 pA (20 ms duration) was used to examine AP properties including resting membrane potential, threshold potential, and rheobase. Firing frequency was examined by measurement of repetitive discharge of each cell on injecting a suprathreshold stimulus of 400 pA for 1000 ms. Measurements obtained from the first AP elicited, with height being the distance from the resting state to the top of the peak and the width as the distance from the initiation of the AP to the most hyperpolarized state. Action potential rising and falling inflections fit to standard exponential function to determine changes in voltage (mV). Time constant (τ) was determined by the following function (f — function, t — sample, Σ — exponential, A — amplitude, i — each component, e — e-fold change, and C — constant y-offset):

$$f(t) = \sum_{i=1}^{n} A_i e^{-t/\tau_i} + C$$

For neuronal current-clamp whole-cell patch recordings, the pipette solution contained the following (in mM): 124 K-gluconate, 2 MgCl2, 13.2 NaCl, 1 EGTA (ethylene glycol-bis(β-aminoethyl ether)-*N,N,N′,N′*-tetraacetic acid), 10 HEPES, pH 7.2. For Chinese hamster ovary (CHO) cell recordings, pipette solution contained (in mM) 130 KCl, 10 NaCl, 1 TEA (tetraethylammonium)-Cl, 20 HEPES, and 5 EGTA, pH 7.2. The external solution contained (in mM) 140 NaCl, 5.4 KCl, 1 CaCl2, 1 MgCl2, 15.6 HEPES, and 10 glucose, pH 7.4. Adult culture recordings with IB4+ dye (Life Technologies) was used to distinguish nonpeptidergic and peptidergic neuron labeling. Cell recordings were excluded if patches were "leaky," observed as a continual drop in resistance after cell break-in.

For the inflammatory model in adult DRG cultures, trinitrophenyl conjugated-lipopolysaccharide (TNP-LPS) conjugate from *Escherichia coli* (List Biological Laboratories, Campbell, CA, USA) was resuspended in media 1 mg/mL and added to cultures (20 µg/mL). Cultures were incubated in 5% CO_2 at 37°C for 10 minutes, washed multiple times, incubated with IB4+ dye, washed multiple times, and immediately recorded. Experiment performed 3 times with multiple coverslips containing neurons.

Site-directed mutagenesis

Site-directed mutagenesis of F834Stop was performed using the PfuTurbo (Agilent Technologies, Santa Clara, CA, USA)–mediated polymerase chain reaction incorporation. rSlick complementary DNA (cDNA) cloned into the expression plasmid pTracer (Invitrogen) was used as the template to introduce mutations. *Dpn*I-digested amplified products were transformed into XL-10 Gold Ultracompetent Cells (Agilent Technologies) and mini-prepped (Qiagen, Hilden, Germany). The plasmids were sequenced for verification. Chinese hamster ovary cells, a gift from L Kaczmarek, Yale University, were transiently transfected with 1.5 µg of either wild-type (WT) or mutated DNA Lipofectamine Reagent (Invitrogen). Cells were recorded 48 hours after transfection, repeated twice.

Statistical analysis

All statistics were performed on Prism 4 (GraphPad Software Inc., La Jolla, CA, USA). All tests were 2-sided, standard error of measure for all measurements. No statistical methods were used to predetermine sample sizes; each method was repeated for validation and until an appropriate sample size was achieved comparable with those reported in our field.

Results

Slick channels are only expressed in a subset of DRG neurons

Neurons within the DRG are heterogeneous in response to varying stimuli, including proprioceptive, nociceptive, mechanoreceptive, thermoceptive, and pruriceptive stimuli.[22] Nociceptive neurons also vary by size and peptide expression. We characterized Slick channel expression in somatic afferent DRG neurons. We imaged using the Axioimager for its large dynamic range, which prevents both saturation of pixels and dim regions from appearing artificially granular. For Slick channel adult mouse IHC studies, strong Slick immunolabeling was identified as punctate within the cytoplasm

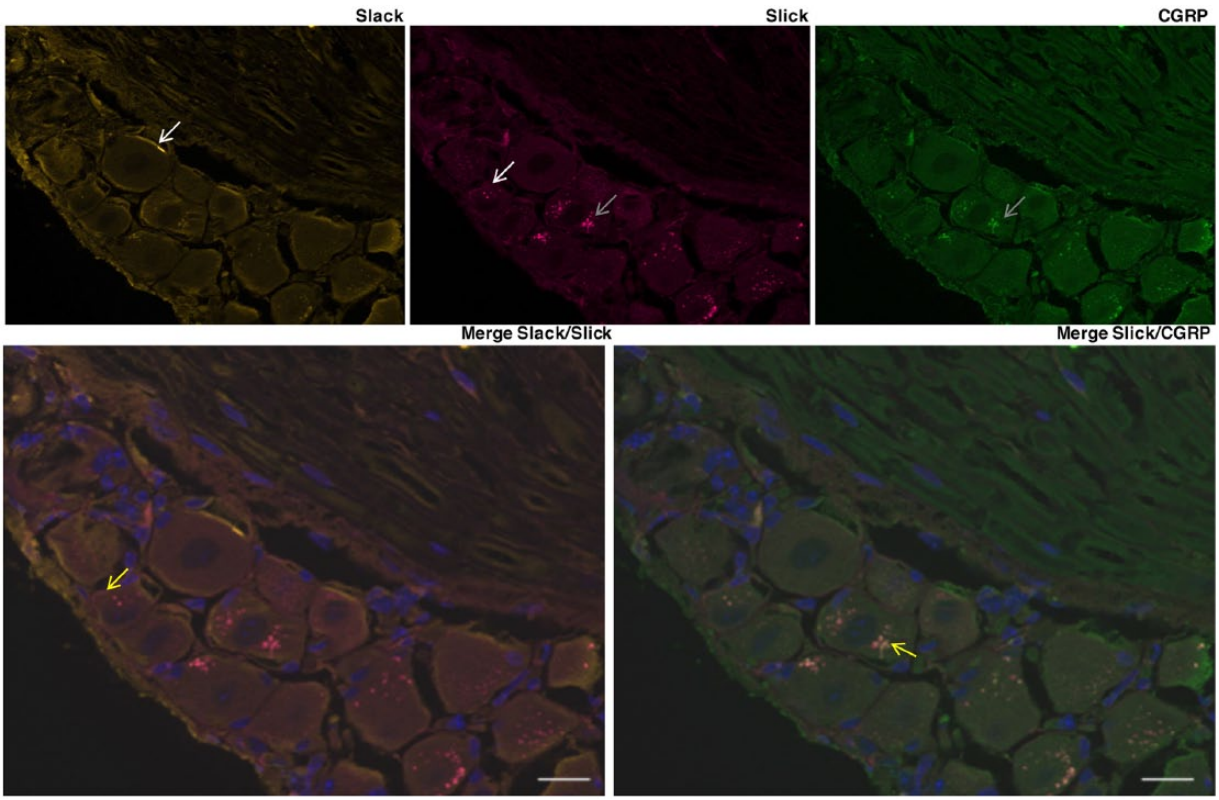

Figure 1. Slick is expressed in a subset of DRG neurons. Representative immunohistochemical images of adult mouse lumbar DRGs immunolabeled for Slack (anti-chicken), Slick (anti-mouse), and CGRP. White arrow—membrane labeling, gray arrow—intracellular labeling, and yellow arrow—co-labeling Slick and Slack (bottom left, orange) or Slick and CGRP (bottom right, yellow). Merge with DAPI. Scale bars: 20 µm. CGRP, calcitonin gene–related peptide; DAPI, 4,6-diamidino-2-phenylindole dihydrochloride; DRG indicates dorsal root ganglion.

of CGRP-positive small-sized and medium-sized lumbar neurons only (Figure 1). Labeling could be detected at the membrane (white arrow), but a substantial proportion of Slick protein was identified intracellularly (gray arrow). More specifically, we observed Slick and CGRP co-immunolabeling within small-sized and medium-sized DRG neurons (yellow arrow). Similar to what was reported previously,[6] and consistent with the Allen Mouse Spinal Cord Atlas (Allen Institute for Brain Science), Slack expression was found throughout mouse lumbar DRG neurons, with most of the immunolabeling localized to the membrane (white arrow) (Figure 1). Slick immunolabeling was also localized to SP-containing lumbar DRG neurons co-expressing CGRP, but Slick immunolabeling was not found in SP-only neurons (Figure S1A). We then analyzed Slick and CGRP immunolabeling in TG sensory neurons. Similarly, we observed Slick and CGRP co-immunolabeling in TG neurons, along with Slick immunolabeling in SP-positive neurons that also contain CGRP (Figure S1B). Slick and CGRP co-immunolabeling was also identified in the spinal cord, the sciatic nerve, and within the paw comprising epidermal tissue and nerve endings (Figure S2). Immunolabeling was more prominent in DRG somas compared with the spinal cord, the sciatic nerve, and the whole paw, likely because the soma is the site of protein synthesis and packaging. Nonetheless, the extrasomal presence of Slick channels suggests that channels function in both stimulus detection (paw) and neurotransmission (spinal cord).

Slick channels are localized to LDCV

Neuropeptides are packaged into LDCV for transportation, release, and volume transmission.[23] Recently, the TRPV1 channel was shown to localize to LDCV-containing CGRP.[24,25] Due to the observed Slick and CGRP co-immunolabeling, we hypothesized that Slick channels are targeted to LDCV-containing CGRP. Sucrose fractionation studies were performed on adult mouse DRGs. Chromogranin-B, a specific LDCV matrix granin, was used to identify and pool LDCV-positive fractions through multiple fractionation steps. Slick protein was detected in the final pooled LDCV-positive fractions, whereas we were unable to identify Slack protein in these same fractions (Figure 2A). To verify Slick localization to LDCV, we performed electron microscopic (EM) studies on adult mouse lumbar DRGs (Figure 2B). Slick antibody was enhanced with DAB for imaging, and control staining was assessed without primary antibody (Figure 2C). Labeling was identified at LDCV within the cell body of small-sized and medium-sized DRG neurons, confirming that Slick channels are targeted to LDCV. We also examined the movement of Slick-containing and CGRP-containing LDCV after stimulation of vesicle release. Embryonic-cultured DRG

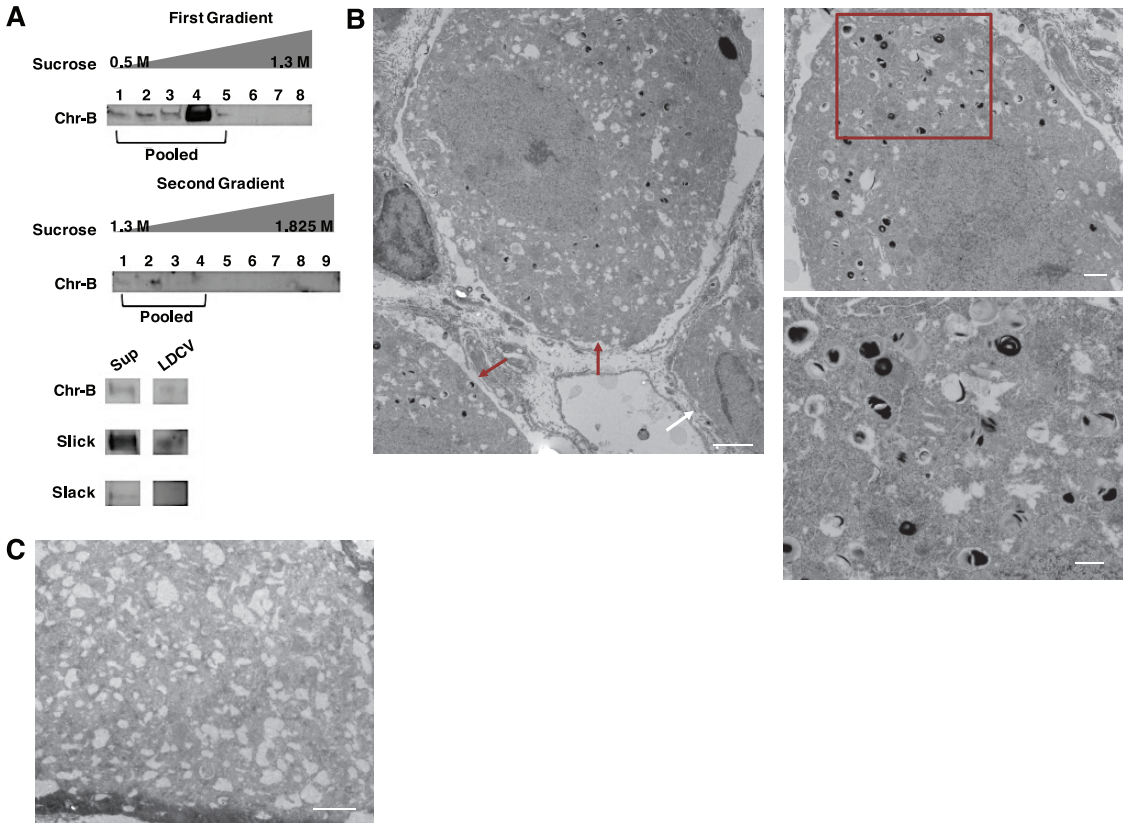

Figure 2. Slick channels are localized to Large Dense-Core Vesicles. (A) LDCV fractionation assay of adult mouse DRGs. Chromogranin-B (Chr-B) used as positive indicator for LDCV. Final pooled elution tested for Chr-B, Slick (anti-mouse), and Slack (anti-mouse) proteins compared to supernatant (Sup) by immunoblot. (B) Representative electron micrography (EM) of adult mouse lumbar DRGs labeled with Slick (anti-mouse) and enhanced with 3,3′-Diaminobenzidine (DAB). Left image indicates staining in small- and medium-sized cell bodies (red arrows), with a nonlabeled cell body (white arrow). Scale bar represents 2 μm (left and top right) and 500 nm (bottom right). Right image enhanced from center image (red box). (C) Representative image of negative control staining adult mouse lumbar DRG no primary with DAB staining. Scale Bar 2 μm.

neurons were depolarized with high (50 mM) KCl to stimulate LDCV docking and release.[26] Using biotinylation assays to immunoprecipitate protein localized to the cell membrane, we identified a near 2-fold increase by semiquantitative measurements in the amount of Slick protein after stimulation with high KCl as compared with low KCl control (Figure 3A). We observed no relative change in the amount of Slack protein at the membrane. Slick and CGRP trafficking to the membrane was also confirmed by immunocytochemistry (ICC) via co-immunolabeling experiments with the surface marker Concanavalin A, following stimulation with high KCl (Figure 3B). The observed movement of CGRP to the DRG neuronal membrane represented a freeze-frame of LDCV movement and docking at the membrane before release of materials, as determined by a colocalization signal (yellow immunofluorescence) of CGRP and Slick. Colocalization, defined as co-occurrence by linear relationship, was determined by Pearson coefficient (Figure 3C). Values are relative to 1, with 1 being the highest linear relationship of 2 fluorescent intensities. We determined a significant increase in Pearson correlation coefficient between CGRP/Con A and Slick/Con A after incubation with high KCl. Together, these results indicate that Slick and CGRP move to the membrane after stimulation of vesicular release.

Validation of previously uncharacterized Slick KO mouse line

A novel and previously uncharacterized Slick reporter global KO mouse line was used to determine the phenotypic consequence of *Slick* deletion. In this mouse model, exons 2 to 7 of *Kcnt2* were replaced with a *LacZ* exon containing a stop codon followed by frameshift in sequence after the exon insertion (Figure 4A), producing a LacZ transgene fused to exon 1. We validated the Slick KO mouse strain by Western blot using whole mouse brain membrane fractions. Mixed strain Slick HET and KO mouse membrane lysates were compared with purebred C57/Bl6 WT mouse membrane lysates. This was performed for initial characterization of the Slick KO mouse line, and all future experiments used littermate controls. Slick protein loss and antibody specificity in Slick KO mice was confirmed (Figure S3A). Next, lumbar DRGs from adult Slick KO mice were isolated and stained for β-galactosidase reactivity. Similar to IHC, LacZ staining was observed only in a proportion of small-sized and medium-sized DRG neurons (Figure 4B). Remarkably, "vesicular" labeling was similar to IHC and EM results (Figures 1 and 2B), suggesting that exon 1, encoding the amino terminal of Slick, controls trafficking to LDCV. LacZ staining was absent in WT DRG (Figure S3B).

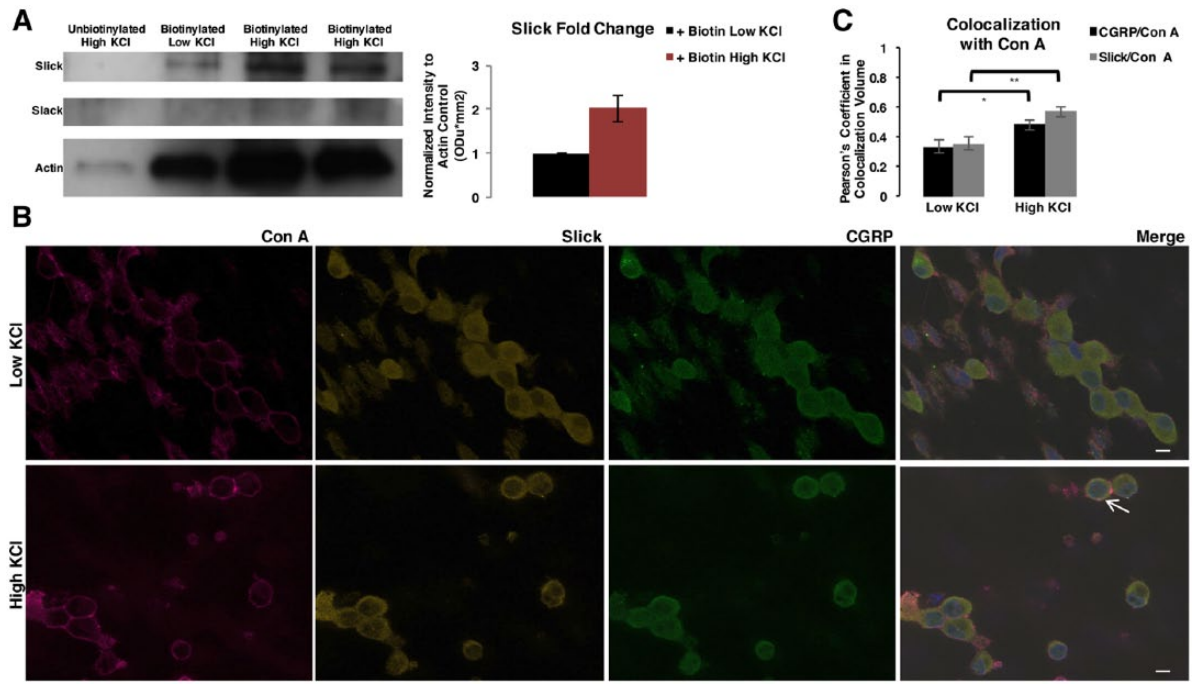

Figure 3. Slick channels move to DRG membrane after large dense-core vesicle stimulation. (A) Biotinylation assay representative blot of cultured embryonic rat DRG neuronal cultures incubated with solution containing low KCl or high KCl for vesicular stimulation for 20 minutes. Two independent replicates for high KCl are indicated in representative blot. Total biotinylated membrane protein probed for Slick (anti-chicken), Slack (anti-mouse), and Actin by immunoblot. Right: Slick intensity normalized to Actin loading control, with low KCl set at 1 Odu*mm^2. Error bars represent SEM. (B) Representative immunocytochemical images of embryonic rat DRG neuronal cultures incubated with solution containing low KCl or high KCl for vesicular stimulation for 20 minutes. Probed with Concanavalin A (Con A) membrane marker, Slick (anti-mouse), and CGRP. Merge with DAPI. Arrow indicates Slick and CGRP colocalization at the membrane with Con A (yellow). Scale bars 20 µm. (C) Quantification of the degree of colocalization by Pearson coefficient. Analysis between CGRP and Con A or Slick and Con A comparing low and high KCl conditions. Statistical analysis by *t* test. $^{**}P \leq .01$; $^{*}P \leq .05$. Error bars represent SEM. DAPI, 4,6-diamidino-2-phenylindole dihydrochloride; DRG, dorsal root ganglia; SEM, standard error of the mean.

There was "vesicular" β-galactosidase staining in the laminar region of the spinal cord and trace amounts in the sciatic nerve and the paw (Figure S4). These results indicate that Slick channels are likely stored and transported to distal sites via LDCV. Finally, to ensure IHC antibody specificity, we stained adult Slick KO mouse DRG. Slick immunolabeling was absent in Slick KO mice (Figure 4C).

Slick KO mice exhibit augmented basal and exacerbated thermal hyperalgesia

Our data suggest that Slick channels may act to counter the effects of heat-dependent and voltage-dependent TRPV1 channels. It was previously shown that TRPV1 agonists cause hypothermia, whereas TRPV1 antagonists cause hyperthermia, and peripheral restriction of these compounds did not alter the drug effects.[27,28] Relative internal temperature was measured noninvasively, and temperature was found significantly decreased in Slick KO compared with WT mice, revealing that Slick KO mice are hypothermic (Figure 5A). Calcitonin gene–related peptide primary sensory neurons encode heat and are unresponsive to mechanical stimuli.[29] Consistent with this phenotype, there were no significant differences in basal mechanical responses by dynamic Von Frey in adult WT and Slick KO mice by either force or time in paw withdrawal latency (Figure 5B). We pursued thermal testing ensuring that phenotypic characterizations represented peripheral properties, that of primary hyperalgesia, as opposed to mechanical allodynia which reflect the contributions of central mechanisms.[30] Baseline behavior was pooled from Hargreaves basal plantar examination over 3 days in WT and Slick KO adult male and female mice. Markedly, Slick KO exhibited augmented basal thermal hyperalgesia in both male and female compared with WT adult mice (Figure 5C). These results suggest that under naïve conditions, some Slick channels are expressed at the DRG neuronal membrane.

The consequences of Slick deletion were further explored in established pain models. We used a neuropathic pain sciatic nerve cuff model of chronic injury, a reversible thermal hyperalgesia model.[20] For an arbitrary set point, we used pooled baseline thermal paw withdrawal latency to assess hyperalgesic recovery. After surgery, cuff-implanted WT mice exhibited increased thermal hyperalgesia, as paw withdrawal latency was significantly lowered day 5 postsurgery. Full recovery was observed day 25 postsurgery compared with pooled baseline (Figure 6A). Cuff-implanted Slick KO mice exhibited exacerbated hyperalgesia and decreased paw withdrawal latency compared with cuff-implanted WT mice, also with paw withdrawal latency significantly lowered day 5

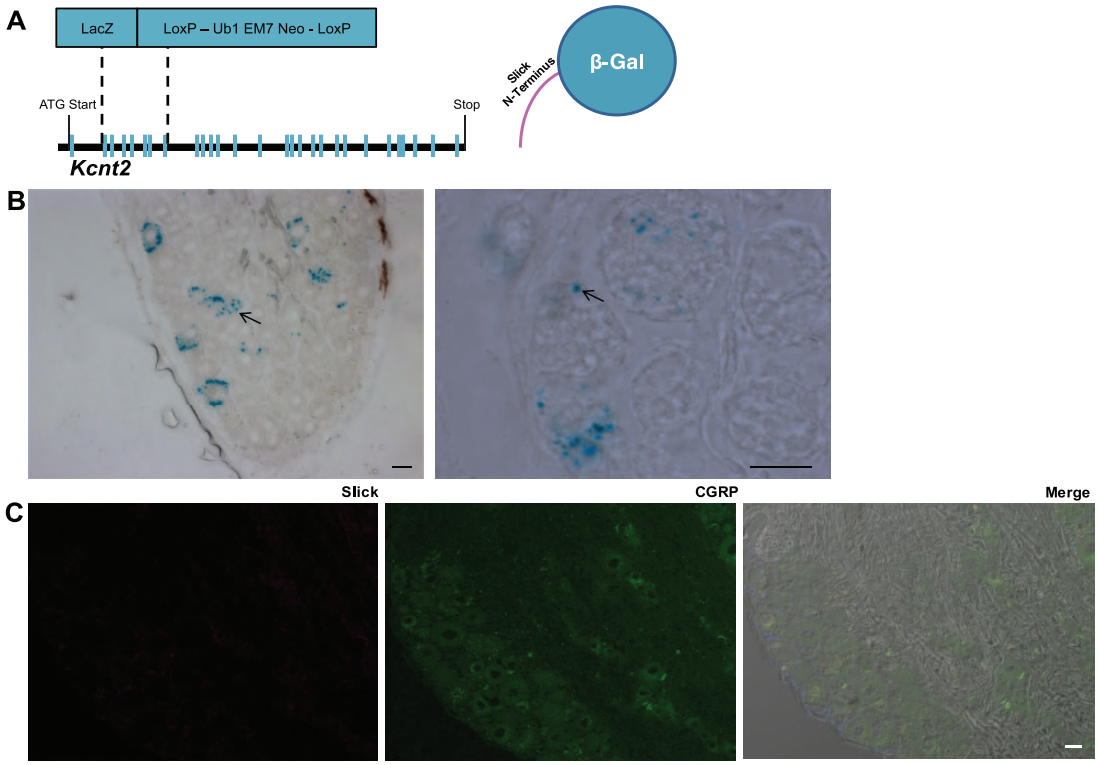

Figure 4. Slick KO mice confirm Slick localization to neuronal subtype. (A) Illustration of Slick-LacZ global KO mice, exons 2 to 7 replaced with LacZ cassette. Right: representation of resultant β-galactosidase protein with partial Slick N-terminal. (B) Representative images of Slick KO mouse DRG X-Gal stain at low and higher magnification. Arrows indicate "punctate X-Gal" staining of the resultant β-galactosidase protein with partial Slick N-terminal. Scale bars: 20 μm. (C) Representative immunohistochemical images of Slick KO mouse DRG exhibiting no Slick (anti-mouse) immunoreactivity. Merge with DAPI and DIC. Scale bars: 20 μm. DAPI, 4,6-diamidino-2-phenylindole dihydrochloride; DIC, differential interference contrast; DRG, dorsal root ganglia; HO, knockout.

postsurgery. Full recovery was also observed day 25 postsurgery compared with pooled baseline. Both male and female mice were tested in each group. No change in paw withdrawal latency was observed in contralateral paw to cuff implantation. To control for estrogen signaling, female mouse samples were tested by vaginal cytology. We identified that females were not synchronized, yet, the pain behavior was consistent between females and overall between male and female mice (Figure S5). Therefore, Slick channels appear to establish the threshold for thermal nociception during neuropathic pain but did not affect the time course for hyperalgesia recovery.

After neuropathic pain experimentation, IHC-stained mid-lumbar DRG neurons were individually selected and analyzed to measure relative integrated density of immunofluorescence. Nerve injury–related cytokines regulate CGRP and nuclear factor κB (NF-κB),[31] and the *Slick* gene is regulated by NF-κB.[19] As may be expected, both Slick and CGRP immunolabeling increased in cuff-implanted WT compared with sham WT mice of DRG neurons (Figure 6B). The increase in both Slick and CGRP immunolabeling indicates that these genes are not only targeted during injury but may also be co-regulated. In Slick KO neurons, CGRP intensity did not change between sham and cuff-implanted WT mice, but relative intensity was significantly lower compared with WT mice. As expected, Slick intensity in adult Slick KO mice was of very low detection and was considered background fluorescence. The relative intensity of SP staining did not change between WT and Slick KO mice (Figure S6A). Cuff-implanted WT mice also exhibited increased levels of Slick and CGRP punctate immunolabeling compared with sham WT mice in sciatic nerve, indicating increased LDCV transport after injury (Figure 6C). We further validated staining using a second Slick antibody and enhanced the signal with DAB (Figure 6D). Slick staining was absent in Slick KO sciatic tissue (Figure S6B). The increased Slick and CGRP immunolabeling in DRG neurons and sciatic nerve after behavioral testing proposes vesicles are targeted to the site of injury.

Slick KO mice display sustained thermal hyperalgesia during inflammatory pain

To test the consequence of Slick deletion in a persistent inflammatory model, we injected CFA into the hind paw of adult male and female mice. For an arbitrary set point, we again used pooled baseline thermal paw withdrawal latency to assess hyperalgesic recovery. Complete Freund's adjuvant–injected WT mice exhibited prolonged but completely reversible thermal hyperalgesia. Paw withdrawal latency was significantly lowered day 1 of testing compared with pooled baseline

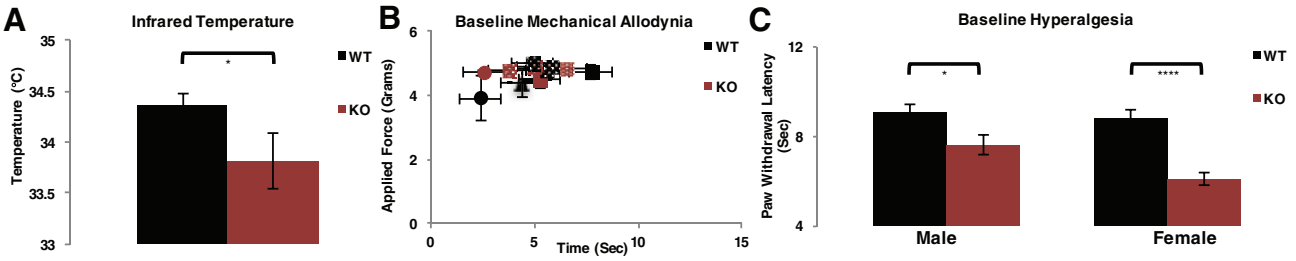

Figure 5. Slick KO mice are hypothermic and exhibit augmented basal hyperalgesia. (A) Infrared temperature measurement of adult Slick male and female mice. (WT: n = 23, KO: n = 13). Statistics by *t* test; error bars represent SEM; **P* ≤ .05. (B) Baseline mechanical measurements in KO and WT female adult mice, WT (all black points) n = 3, KO (all red points) n = 3. Each point represents left or right hind paw averaged measurements from behavioral testing each day, over a 3-day testing period. (C) Combined thermal baseline response of both paws from Hargreaves plantar test of adult Slick male and female mice. Male, WT: n = 10, KO: n = 8; female WT: n = 16, KO: n = 15. Statistics by *t* test; error bars by SEM. *****P* ≤ .0001; **P* ≤ .05. KO indicates knockout; SEM, standard error of the mean; WT, wild type.

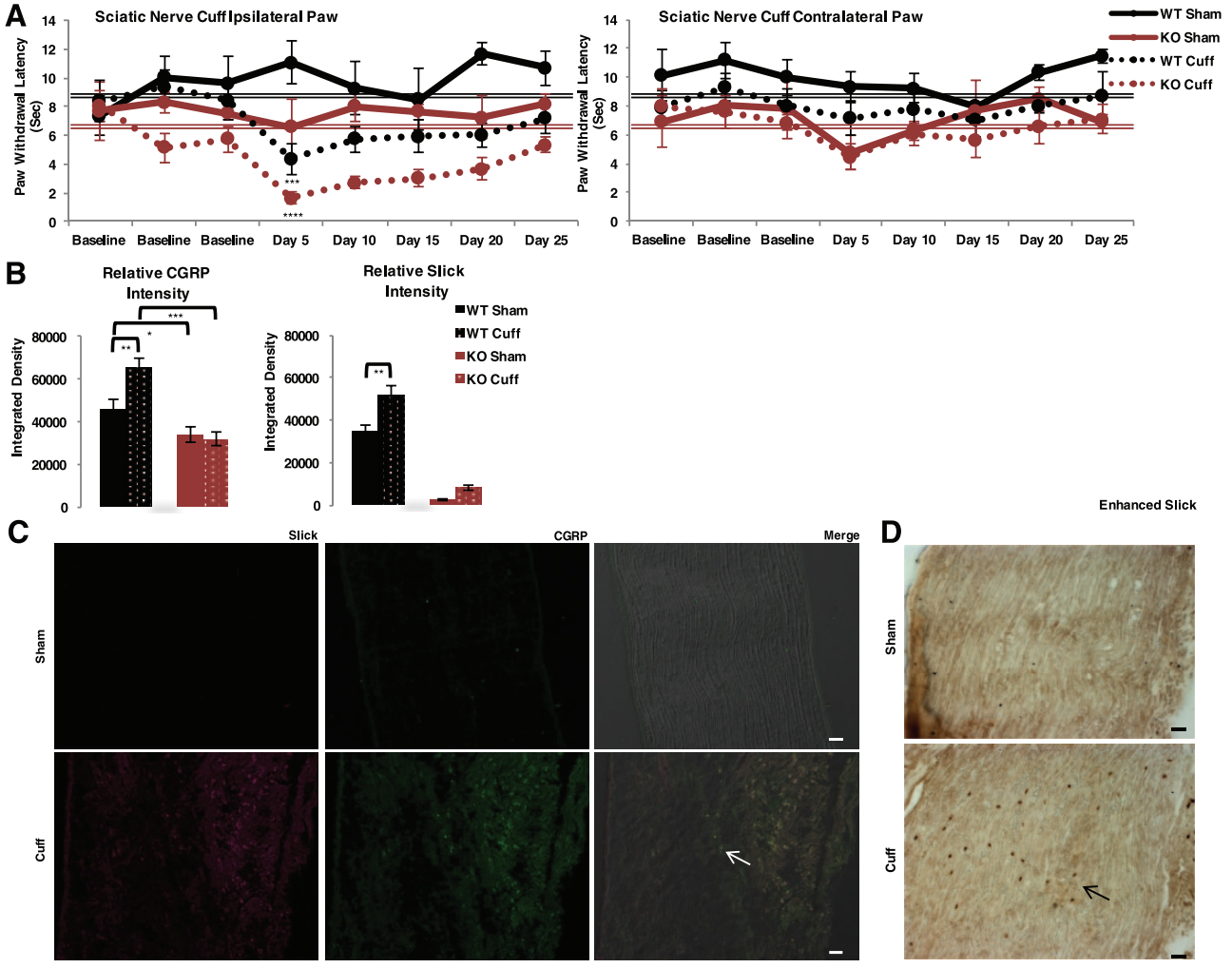

Figure 6. Slick KO mice demonstrate exacerbated thermal hyperalgesia during neuropathic pain model. (A) Hargreaves plantar test of sciatic nerve cuffing model adult Slick WT and KO male and female mice. Ipsilateral paw to the injured nerve and contralateral paw to injured nerve. WT Sham: n = 4, WT Cuff: n = 7, KO Sham: n = 4, and KO Cuff: n = 7. Statistics by 2-way ANOVA multiple comparisons RM; significant difference in both genotype and condition. For comparison of each testing day to average pooled baseline measurements from Figure 5C (WT [double black line], KO [double red line]), statistics by *t* test. *****P* ≤ .0001; ***P* ≤ .01. (B) Fluorescent quantification of individually isolated lumbar DRG soma Slick (anti-mouse) and CGRP immunoreactivity by IHC after behavioral examination. Number of cells analyzed per condition: WT Sham; CGRP: n = 26, Slick: n = 26, WT Cuff; CGRP: n = 143, Slick: n = 143, KO Sham; CGRP: n = 43, Slick: n = 43, KO Cuff; CGRP: n = 47, Slick: n = 47. Statistics by 1-way ANOVA. ****P* ≤ .001; ***P* ≤ .01; **P* ≤ .05. Error bars represent standard error of the mean. (C) Representative IHC of sciatic nerve from sham and cuff mice post behavior indicating increase in Slick (anti-mouse) and CGRP immunoreactivity in cuff mice. Arrow indicates merged Slick and CGRP (yellow). (D) Representative image of sciatic nerve from sham and cuff mice with Slick (anti-chicken) antibody enhanced with DAB. Scale bars 20 µm. ANOVA indicates analysis of variance; CGRP, calcitonin gene–related peptide; IHC, immunohistochemistry; KO, knockout; WT, wild type.

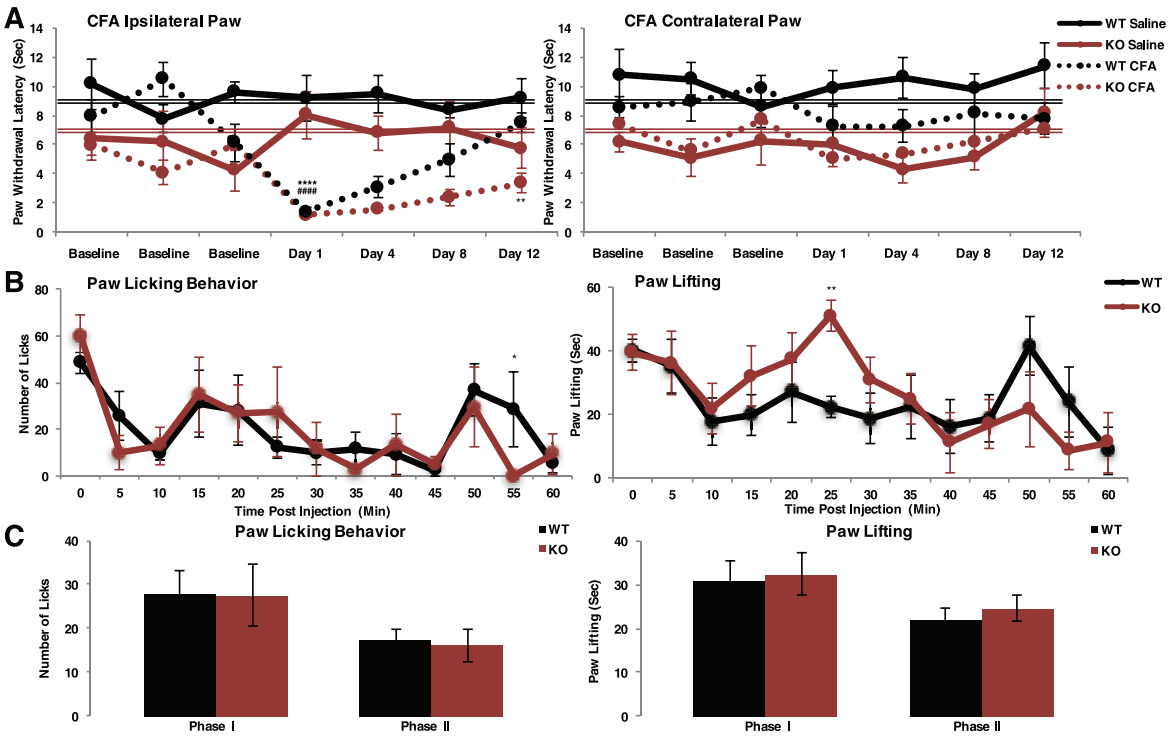

Figure 7. Slick KO mice exhibit sustained thermal hyperalgesia during chronic inflammatory model. (A) Hargreaves plantar test of persistent inflammatory pain model of complete Freund's adjuvant (CFA) injection into the hind paw of male and female adult Slick mice. Ipsilateral paw to the injected paw and contralateral paw to the uninjected paw. WT Saline: n=5, WT CFA: n=7, KO Saline: n=4, KO CFA: n=5. Statistics by 2-way ANOVA multiple comparisons RM; significant difference in both genotype and condition. For comparison of each testing day to average pooled baseline measurements from Figure 5C (WT [double black line], KO [double red line]), statistics by *t* test. *WT, #KO. $^{**}P \leq .01$; $^{****}P \leq .0001$. (B and C) Formalin acute inflammatory model for nocifensive behavior. (B) Average licking and lifting behavior scored per minute over 60 minutes. (C) Average behavior grouped between Phase I (0-10 minutes) and Phase II (15-60 minutes). Statistics by 2-way ANOVA multiple comparisons RM least significant difference. Error bars by SEM. *WT vs KO: $^{**}P \leq .01$; $^{*}P \leq .05$. ANOVA indicates analysis of variance; KO, knockout; SEM, standard error of the mean; WT, wild type.

measurements, with recovery to baseline day 12 (Figure 7A). Conversely, CFA-injected Slick KO mice exhibited an intensified thermal hyperalgesic response that failed to recover after 12 days of testing. Day 12 paw withdrawal latency remained significantly lower than baseline measurements. No change in paw withdrawal latency was observed in contralateral paw to cuff implantation. Slick channels are therefore essential for the thermal hyperalgesic recovery during persistent inflammation. After behavioral testing, injected paws were analyzed for Slick and CGRP immunolabeling. Whole paw staining indicated Slick and CGRP punctate staining increased in WT CFA-injected paw compared with WT saline control, suggesting that part of the CFA recovery process involves an increased synthesis and transport of CGRP and Slick channel–containing LDCV to the sight of inflammation at the axon terminal (Figure S7). Calcitonin gene–related peptide punctate staining was decreased in Slick KO CFA-injected paw. We then probed hind paw edema by caliper measurement. Although there was an observed increase in edema of CFA-treated Slick KO mice compared with WT mice 1 day after injection, it did not reach the level of significance (Figure S8). By the end of the behavioral study, hind paw size did not differ between mice. The similar hind paw edema at the end of behavioral examination suggests that the sustained behavioral response in Slick KO mice was likely due to a persistent altered excitability. Slick channels are found important for the recovery process after chronic inflammatory injury.

We sought to differentiate between peripheral and central nociceptive contributions in our global Slick KO mouse line. The established formalin model provides the ability to define peripheral mechanisms by scoring nocifensive behavior after acute inflammation. We found no statistical difference between WT and Slick KO adult male and female mice in phase I nor phase II nocifensive behavior, including licking behavior or time spent lifting paw (Figure 7B and C). The lack of a significant formalin behavioral response in Slick KO mice is similar to TRPV1 KO mouse formalin behavior.[32,33] The formalin data indicated that central pain processing is in fact intact in Slick KO mice and that the hyperalgesic responses observed are primarily peripherally based.

Decreased outward potassium current and altered AP properties in DRG neurons from Slick KO mice

To determine the electrophysiologic consequence of Slick channel loss, we used whole-cell voltage-clamp and current-clamp techniques to investigate current and excitability properties in DRG sensory neurons. We first analyzed the properties of

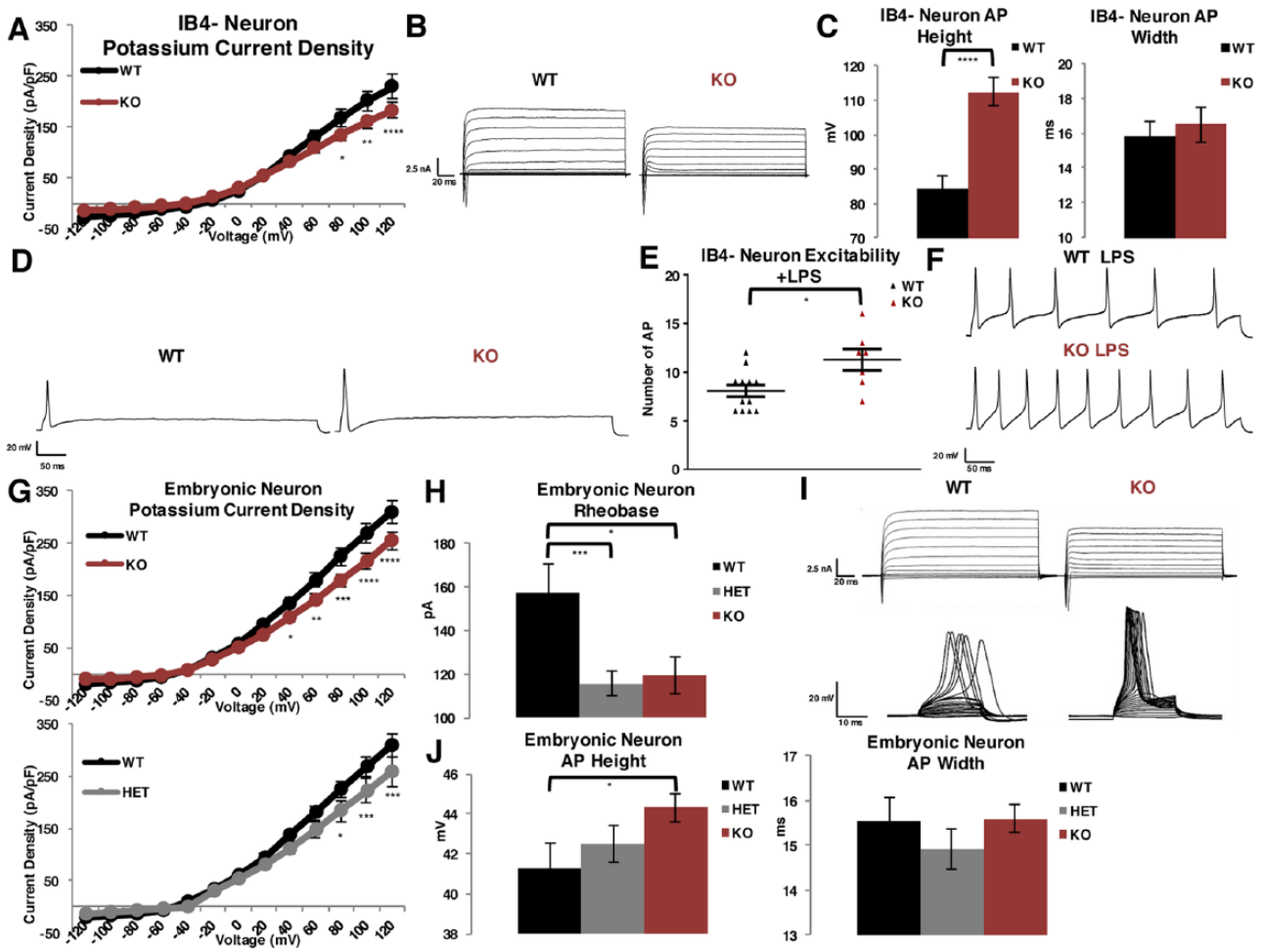

Figure 8. Decreased outward potassium current and altered AP properties in DRG neurons from Slick KO mice. (A-E) Adult mouse cultured neurons. (A) Current densities of outward potassium current in cultured small and medium peptidergic IB4– DRG neurons isolated from adult male and female mice taken from 150 ms of the depolarizing step. Voltage-clamp whole-cell recordings were obtained from WT and KO neurons cultured in nerve growth factor after 3 days (n = 38). (B) Representative traces of total outward currents. (C) Measurement of average AP height and width on 2.5× suprathreshold stimulus at 400 pA for 1000 ms, WT: n = 31, KO: n = 32. (D) Representative traces of single AP elicited after 400 pA suprathreshold stimulus over 1000 ms in WT vs KO neurons. (E) Hyperexcitable neuronal response after incubation with LPS between WT and KO IB4– neurons on 2.5× suprathreshold stimulus at 400 pA for 1000 ms, WT: n = 12, KO: n = 7. (F) Representative traces of hyperexcitable neurons after LPS stimulation. (G-J) Embryonic mouse cultured neurons. (G) Current densities measured in WT: n = 14, HET: n = 18, and KO: n = 23 neurons cultured 10 to 13 days. (H) Current required to generate AP (rheobase) WT: n = 11, HET: n = 18, and KO: n = 21 neurons. AP from current-clamp whole-cell recordings. (I) Representative traces of total outward current (above) and injection of current to achieve rheobase (below). (J) Measurement of height and width of APs from WT: n = 18, HET: n = 29, and KO: n = 35 neurons. Current density statistics by multiple comparisons *t* test, AP height and width, excitability, and rheobase by *t* test. **P* ≤ .05; ***P* ≤ .01; ****P* ≤ .001; *****P* ≤ .0001. Error bars by SEM. AP indicates action potential; DRG, dorsal root ganglia; HET, heterozygous; KO, knockout; LPS, lipopolysaccharide; SEM, standard error of the mean; WT, wild type.

dissociated peptidergic adult DRG neurons from Slick KO and WT mice. There was a significant decrease in total outward potassium current in IB4– Slick KO neurons compared with WT (Figure 8A and B). After further investigation into AP properties, we determined that dissociated neurons exhibited similar firing patterns between Slick KO IB4– compared with WT IB4– neurons. We observed 4 groups of excitability levels, nonresponders that did not fire APs, a group that fired 1 AP, a group that fired more than 1 AP, and a hyperexcitable group that fired more than 5 APs. We report there was no significant difference in AP numbers (Table S1). However, Slick IB4– KO neurons that fired exhibited a prominent increase in AP height, with no change in AP width compared with WT IB4– neurons (Figure 8C and D). Next, we examined the inflections of the APs. At random, we chose 6 neurons that fired 1 AP and measured inflection slopes fit to an exponential standard function to define τ. We report no significant difference in rising nor falling inflection slopes between WT and Slick KO IB4– neuronal APs (Table S1). To investigate the contribution of Slick channels to repetitive firing, we treated neurons with an inflammatory mediator that both promotes CGRP release and excites neurons. We incubated neurons with *E coli* derived lipopolysaccharide (LPS), a classical inflammatory signaling response wherein LPS binds toll-like receptor 4 causing downstream activation of cytokines and cyclooxygenase-dependent prostanoid production.[34] Toll-like receptor 4 is found in both peptidergic and nonpeptidergic neurons of the DRG.[35] Lipopolysaccharide is also found to evoke CGRP release and

elevate intracellular calcium in cultured DRG neurons.[36] All neurons exhibited multiple AP firing after stimulation with LPS, but we identified a significant increase in the number of APs in IB4– Slick KO neurons compared with IB4– WT neurons (Figure 8E and F). Finally, to verify that Slick channels are restricted to peptidergic neurons, we then recorded IB4+-labeled DRG neurons. We found no significant difference in outward potassium current density nor AP height and width between WT and Slick KO IB4+ neurons. (Figure S9). These results confirm Slick channels are expressed primarily in IB4– peptidergic DRG neurons.

We then examined cultured embryonic DRG neurons, a more ideal system for our studies owing to the homogeneous firing properties, stable resting membrane potentials, and predominantly peptidergic population of these neurons.[7] Moreover, IB4+ labeling and its potential confounding effects is eliminated when probing these cultures. In agreement with adult cultured peptidergic IB4– neurons, we found Slick KO potassium currents are reduced as compared with WT currents (Figure 8G and I). Furthermore, neurons isolated from HET mice showed a reduced yet significant decrease in current, demonstrating gene-dosing effects. A prominent decrease in rheobase, the minimum injection of current needed to elicit an AP, was detected in Slick HET and Slick KO neurons compared with WT neurons (Figure 8H and I). The significant increase in AP height was validated in Slick KO neurons compared with WT neurons (Figure 8J). We again examined the inflections of the neurons, selecting 6 neurons at random and measuring inflection slopes fit to an exponential standard function to define τ. We report no significant difference in rising and falling inflection slopes between WT, Slick HET, and Slick KO neuronal APs (Table S1). Together, the electrophysiologic properties indicated Slick channels contribute to outward current, are essential in restraining AP height, decrease propensity to fire APs, and limit excitability during inflammatory provocation.

Investigation into previously reported Slick KO mouse line

Previous studies using a different *Slick* (*Slo2.1*) KO mouse line did not report a pain phenotype.[10] In this prior investigation, studies were focused on nonpeptidergic IB4+ neurons. Importantly, their transgenic line was made by deleting exon 22, producing a stop codon in the second regulator of K+ conductance (RCK) domain in the distal C-terminus and leaving the transmembrane domains, the pore region and RCK domain 1, intact. To mimic this Slick transgene, we engineered a truncation stop codon (F834Stop), representing loss of exon 22 in a rat Slick cDNA construct. Upon performing whole-cell voltage-clamp recordings on transfected CHO cells, we were able to detect outward-rectifying potassium currents that partially gated (Figure S10), underscoring the fact that the channels can still assemble. To further support this notion, we then performed ICC comparing the Slick WT with F834Stop mutation with pTracer empty vector. The epitope for the antibody is still present in the F834Stop truncated channel. The pTracer bicistronic vector expresses green fluorescent protein (GFP). By ICC, we detected Slick WT and F834Stop mutated channels in GFP expressing cells, whereas no immunolabeling was detected in pTracer empty vector–transfected cells (Figure S11). At least in heterologous expression systems, the truncated Slick protein is stable. This could be important because partial Slack C-terminal protein products were previously identified by *in vitro* translation assay.[5] Consequently, these products containing RCK domains may be interacting with the truncated Slick channel to produce fully functional channels in this mouse line. Still, the authors previously reported an absence of the truncated Slick protein by Western analyses of brain membrane fractions and suggested that the absence may have been due to protein instability,[10] despite a lack of IHC studies. The investigators only detected significant pain behavior in Slick– Slack– double KO mice and suggested that Slick and Slack channels exist as heterotetramers. If this were the case, the unstable truncated Slick channel in their Slick transgenic mouse line should have produced a dominant negative effect on Slack channel expression, and therefore, a similar pain behavior should have been detected in Slick-only KO mice. Our data suggests that Slick channels can assemble as homotetramers and act independently of Slack channels, at the very least those channels that are targeted to and stored in LDCV.

Discussion

Slick channels act to restrain CGRP+ nociceptive DRG neurons

We are the first to report a physiologic role for Slick channels in DRG neurons. Slick channels were localized to CGRP-containing neurons only (Figure 1). Slick protein synthesis appeared to primarily occur at DRG soma, where LDCVs are sorted, and channels are transported via LDCV to the periphery as indicated by the punctate staining within the sciatic nerve, the spinal cord, and the nerve ending at the paw (Figures 4B, 6C and D; Figures S2, S4, and S7). Slick KO mice displayed both hypothermia and augmented basal hyperalgesia (Figure 5A and C). Furthermore, the consequence of Slick channel loss was indicated by an exacerbated thermal hyperalgesic response to neuropathic pain (Figure 6A) and a sustained thermal hyperalgesic response to persistent inflammatory pain (Figure 7A). These effects were found primarily peripherally based (Figure 7B and C). In peptidergic DRG neurons, Slick channels contributed to outward potassium current but importantly acted to regulate the AP height, propensity to fire APs, and increased excitability during inflammatory signaling (Figure 8).

Slick channels shape AP properties

The electrophysiologic properties of Slick channels and their contribution to firing properties in DRG neurons corroborated the hyperalgesic behavioral phenotype we observed in Slick KO

mice. The most salient feature we observed after Slick channel loss was the significant increase in AP height in both peptidergic adult and embryonic DRG neurons. In addition, we observed no changes in time constant during the repolarization phase of the AP. An augmentation in AP height could have multiple effects on pain signaling. Temporally, it was observed that calcium currents in small-sized and medium-sized DRG neurons initiate at the peak of the AP, likely due to the slower activation kinetics of calcium channels.[37] Theoretically then, the increased AP height in Slick KO DRG neurons, with no change in time constant during repolarization, would mean that in these neurons a significant increase in calcium accumulation occurs during AP repolarization. This would affect neurotransmission and signaling cascades. As we observed Slick-positive and CGRP-positive LDCV at the level of the spinal cord, we expect Slick channels to reside at presynaptic terminals. We infer that an enhanced AP height would likely result in elevated neurotransmitter release at the spinal cord synapses, providing an explanation to the observed increased basal thermal responsiveness in Slick KO mice. Furthermore, a characterization of C-fiber AP properties uncovered positive correlation between IB4 intensity and increased AP height in C-fibers.[38] This finding suggests a necessary biologically conserved mechanism in restraining AP height in nociceptive peptidergic neurons. Another consequence of increased AP height could be an increase in activation of TRPV1 channels. In addition to heat and acid, TRPV1 channels are gated at higher membrane voltages (voltages that reach the reversal potential of sodium).[39] Even small changes in AP height would have a profound influence on TRPV1 open probability.[39] Consequently, limiting AP height would therein reduce TRPV1 channel activity. Colocalization of Slick channels with TRPV1 channels[25,26] to LDCV in CGRP-containing nociceptors and their presumed co-migration to the membrane during pain is supported by our observations that hyperalgesic pain was exacerbated and prolonged during chronic pain in Slick KO mice.

We suggest that Slick channels limit AP height by their unique fast activation properties. In addition, there are 2 other fundamental properties of Slick channels that explain why channels only contribute to AP height. First, Slick channels are weakly voltage-dependent.[40] At lower concentrations of the Slick channel activator niflumic acid, the G-V relationship was observed to be $V_{1/2}$ of +95 mV but did shift to more negative voltages at higher concentrations of the drug. The weak voltage dependence would explain the observed significant reduction in current density at more positive voltages (Figure 8) we observed in our recording conditions. Second, Slick channels are weakly sodium dependent, with an EC_{50} for sodium that is more than double of what is observed for Slack channels.[12] In combination, the fast activation, weak voltage, and sodium dependence predict that channels are most active during the peak of the AP when sodium accumulation and voltage are at their highest.

We identified that Slick channels also increase AP firing threshold, at least in peptidergic embryonic neurons. We did not observe rheobase changes in adult DRG neurons, but this may be the result of the heterogeneity and instability of electrogenic properties within dissociated neurons. It could be that during small depolarizations, sodium and chloride influx can open a few Slick channels affecting rheobase. This may be contributing to the set point for basal nociception to thermal stimuli in both male and female mice, as Slick channels were localized to nerve endings in the periphery (Figure S2 and 7). Slick channel loss was also found to increase AP number in the presence of the inflammatory mediator LPS and this observation correlates with the inability for Slick KO mice to recover to baseline during CFA-induced inflammation. We are proposing that Slick channels act as counterweights, behaving as moderators of nociception by limiting AP height and restraining excitability in CGRP-containing nociceptive neurons.

Slick and CGRP are co-regulated genes

The restricted expression of Slick channels to peptidergic CGRP neurons and their effects on nociceptor excitability emphasizes their specialized function in controlling hyperalgesic behavior. The central role of CGRP in pain and inflammation, along with the pain modality that CGRP neurons encode,[29] makes it plausible that these neurons would evolve to express a precise set of molecules that can restrain activity. As we have presented in our data, it appears that the expression of CGRP and Slick channels is in sync. Both genes are likely regulated by inflammatory cytokines, notably Slick via NF-κB signaling.[19] *Slick* and *CGRP* expression was found increased in parallel in DRG neurons of *Runx1* conditional KO mice, lacking the Runx1 transcription factor essential for the specification of a large cohort of sensory neurons involved in pain, itch, and temperature sensation.[41] This study indicated that *Slick* and *CGRP* expressions were found in DRG neurons that innervated mesodermal and endodermal tissue and suggests that Slick and CGRP are important in deep tissue pain. Together, *CGRP* and *Slick* emerge as co-regulated genes.

Calcitonin gene–related peptide has garnered particular attention as a therapeutic target to treat a number of debilitating human diseases including migraines, ulcerative colitis, neuropathic pain, arthritis, and asthma.[42–46] Calcitonin gene–related peptide also contributes to neurogenic inflammation and to the development and maintenance of central sensitization after peripheral injury.[47] Calcitonin gene–related peptide binds to G-coupled protein receptor calcitonin receptor–like receptor (CLR), and CLR requires binding of the associated proteins receptor activity-modifying protein 1 and receptor component protein for a fully functional receptor.[48] However, GPCRs have the ability to bind other accessory proteins to alter functionality. Owing to the promiscuity of these GPCRs, directly antagonizing the CGRP receptor has been problematic, but CGRP-directed antibodies for pain treatment have shown clinical promise.[49] Targeting Slick channels to specifically limit

CGRP peptide release could represent an alternative therapeutic strategy over broadly targeting GPCRs. Moreover, the specific Slick expression in CGRP-expressing neurons underscores their potential as therapeutic candidates for pain.

The phenotypic effects we have observed in Slick KO mice indicate that there may also be humans with erroneously functioning channels naïve to their complications. Sulem et al[50] reported on isolated homozygous and compound HET loss-of-function mutations on a variety of genes, which included *KCNT2* in an Icelandic population. Asthma, arthritis, and migraines were among the most prevalent diseases associated with this population. Going forward, *KCNT2* channelopathies should be scrutinized when screening inflammatory and pain-related diseases.

Acknowledgements

The authors would first like to thank Dr Karen C Dietz for help in establishing Slick KO mouse colony and initial characterization; students David Personius and Garrett D Sheehan for their time scoring mice for formalin behavioral examination; Dr Shannon J Clough, who was instrumental to determining vaginal cytology and assistance with formalin model; and Dr Wade J Sigurdson, for assistance in IHC imaging and analysis. They would also like to thank Jasmine Lopez for assistance in measuring mouse infrared temperature. Finally, they would like to thank Dr Malcolm Slaughter for help with the AP analyses.

Author Contribution

DLT and AB designed the study, interpreted results and wrote the manuscript. DLT performed all experiments, including the perfusion and staining of adult mouse DRG for electron microscopy. EH and LW went on to process tissue and perform electron microscopy.

Data Availability

The authors declare that all data supporting the findings of this study are available within the article and its supplementary information. Raw data and formalin behavioral videos are available on appropriate request from corresponding author.

REFERENCES

1. Benarroch EE. Ion channels in nociceptors: recent developments. *Neurology*. 2015;84:1153–1164.
2. Kruger L, Sternini C, Brecha NC, Mantyh PW. Distribution of calcitonin gene-related peptide immunoreactivity in relation to the rat central somatosensory projection. *J Comp Neurol*. 1998;273:149–162.
3. Tsantoulas C, McMahon SB. Opening paths to novel analgesics: the role of potassium channels in chronic pain. *Trends Neurosci*. 2014;37:146–158.
4. Kaczmarek LK. Slack, Slick and sodium-activated potassium channels. *ISRN Neurosci*. 2013;2013:354262.
5. Bhattacharjee A, Gan L, Kaczmarek LK. Localization of the Slack potassium channel in the rat central nervous system. *J Comp Neurol*. 2002;454:241–254.
6. Tamsett TJ, Picchione KE, Bhattacharjee A. NAD+ activates KNa channels in dorsal root ganglion neurons. *J Neurosci*. 2009;29:5127–5134.
7. Nuwer MO, Picchione KE, Bhattacharjee A. PKA-induced internalization of slack KNa channels produces dorsal root ganglion neuron hyperexcitability. *J Neurosci*. 2010;30:14165–14172.
8. Huang F, Wang X, Ostertag EM, et al. TMEM16C facilitates Na(+)-activated K+ currents in rat sensory neurons and regulates pain processing. *Nat Neurosci*. 2013;16:1284–1290.
9. Lu R, Bausch AE, Kallenborn-Gerhardt W, et al. Slack channels expressed in sensory neurons control neuropathic pain in mice. *J Neurosci*. 2015;35:1125–1135.
10. Martinez-Espinosa PL, Wu J, Yang C, et al. Knockout of Slo2.2 enhances itch, abolishes KNa current, and increases action potential firing frequency in DRG neurons. *ELife*. 2015;4:10013.
11. Joiner WJ, Tang MD, Wang LY, et al. Formation of intermediate-conductance calcium-activated potassium channels by interaction of Slack and Slo subunits. *Nat Neurosci*. 1998;1:462–469.
12. Bhattacharjee A, Joiner WJ, Wu M, Yang Y, Sigworth FJ, Kaczmarek LK. Slick (Slo2.1), a rapidly-gating sodium-activated potassium channel inhibited by ATP. *J Neurosci*. 2003;23:11681–11691.
13. Suzuki T, Hansen A, Sanguinetti MC. Hydrophobic interactions between the S5 segment and the pore helix stabilizes the closed state of Slo2.1 potassium channels. *Biochim Biophys Acta*. 2016;1858:783–792.
14. Tejada MA, Stople K, Hammami Bomholtz S, Meinild AK, Poulsen AN, Klaerke DA. Cell volume changes regulate slick (Slo2.1), but not slack (Slo2.2) K+ channels. *PLoS ONE*. 2014;9:e110833.
15. Bhattacharjee A, von Hehn CA, Mei X, Kaczmarek LK. Localization of the Na+-activated K+ channel Slick in the rat central nervous system. *J Comp Neurol*. 2005;484:80–92.
16. Rizzi S, Knaus H-G, Schwarzer C. Differential distribution of the sodium-activated potassium channels slick and slack in mouse brain. *J Comp Neurol*. 2016;524:2093–2116.
17. Bansal V, Fisher TE. Na+-activated K+ channels in rat supraoptic neurons. *J Neuroendocrinol*. 2016;28:6.
18. Zhao B, Wang HB, Lu YJ, Hu JW, Bao L, Zhang X. Transport of receptors, receptor signaling complexes and ion channels via neuropeptide-secretory vesicles. *Cell Res*. 2011;21:741–753.
19. Tomasello DL, Gancarz-Kausch AM, Dietz DM, Bhattacharjee A. Transcriptional regulation of the sodium-activated potassium channel SLICK (KCNT2) promoter by nuclear factor-κB. *J Biol Chem*. 2015;290:18575–18583.
20. Yalcin I, Megat S, Barthas F, et al. The sciatic nerve cuffing model of neuropathic pain in mice [published online ahead of print July 16, 2014]. *J Vis Exp*. doi:10.3791/51608.
21. Byers SL, Wiles MV, Dunn SL, Taft RA. Mouse estrous cycle identification tool and images. *PLoS ONE*. 2012;7:e.35538.
22. Basbaum AI, Bautista DM, Scherrer G, Julius D. Cellular and molecular mechanisms of pain. *Cell*. 2009;139:267–284.
23. Thureson-Klein Å, Stjärne L. Dense cored vesicles in actively secreting noradrenergic neurons. In: Stjärne L, Hedqvist P, Lagercrantz H and Wennmalm A, eds. *Chemical Neurotransmission 75 Years*. London, England: Academic Press; 1981:153–164.
24. Devesa I, Ferrándiz-Huertas C, Mathivanan S, et al. αCGRP is essential for algesic exocytotic mobilization of TRPV1 channels in peptidergic nociceptors. *Proc Natl Acad Sci U S A*. 2014;111:18345–18350.
25. Meng J, Wang J, Steinhoff M, Dolly JO. TNFα induces co-trafficking of TRPV1/TRPA1 in VAMP1-containing vesicles to the plasmalemma via Munc18-1/syntaxin1/SNAP-25 mediated fusion. *Sci Rep*. 2016;6:21226.
26. Ai X, MacPhedran SE, Hall AK. Depolarization stimulates initial calcitonin gene-related peptide expression by embryonic sensory neurons in vitro. *J Neurosci*. 1998;18:9294–9302.
27. Gavva NR. Body-temperature maintenance as the predominant function of the vanilloid receptor TRPV1. *Trends Pharmacol Sci*. 2008;29:550–557.
28. Romanovsky AA. Thermoregulation: some concepts have changed. Functional architecture of the thermoregulatory system. *Am J Physiol Regul Integr Comp Physiol*. 2007;292:R37–R46.
29. McCoy ES, Taylor-Blake B, Street SE, Pribisko AL, Zheng J, Zylka MJ. Peptidergic CGRPα primary sensory neurons encode heat and itch and tonically suppress sensitivity to cold. *Neuron*. 2013;78:138–151.
30. Treede RD, Meyer RA, Raja SN, Campbell JN. Peripheral and central mechanisms of cutaneous hyperalgesia. *Prog Neurobiol*. 1992;38:397–421.
31. Bowen EJ, Schmidt TW, Firm CS, Russo AF, Durham PL. Tumor necrosis factor-alpha stimulation of calcitonin gene-related peptide expression and secretion from rat trigeminal ganglion neurons. *J Neurochem*. 2006;96:65–77.
32. Bölcskei K, Helyes Z, Szabó A, et al. Investigation of the role of TRPV1 receptors in acute and chronic nociceptive processes using gene-deficient mice. *Pain*. 2005;117:368–376.
33. Staniland AA, McMahon SB. Mice lacking acid-sensing ion channels (ASIC) 1 or 2, but not ASIC3, show increased pain behaviour in the formalin test. *Eur J Pain*. 2009;13:554–563.
34. Tse KH, Chow KB, Leung WK, Wong YH, Wise H. Lipopolysaccharide differentially modulates expression of cytokines and cyclooxygenases in dorsal root ganglion cells via Toll-like receptor-4 dependent pathways. *Neuroscience*. 2014;267:241–251.
35. Due MR, Piekarz AD, Wilson N, et al. Neuroexcitatory effects of morphine-3-glucuronide are dependent on Toll-like receptor 4 signaling. *J Neuroinflammation*. 2012; 9:200.

36. Hou L, Wang X. PKC and PKA, but not PKG mediate LPS-induced CGRP release and [Ca(2+)](i) elevation in DRG neurons of neonatal rats. *J Neurosci Res*. 2001;66:592–600.
37. Scroggs RS, Fox AP. Multiple Ca2+ currents elicited by action potential waveforms in acutely isolated adult rat dorsal root ganglion neurons. *J Neurosci*. 1992;12:1789–1801.
38. Fang X, Djouhri L, McMullan S, et al. Intense isolectin-B4 binding in rat dorsal root ganglion neurons distinguishes C-fiber nociceptors with broad action potentials and high Nav1.9 expression. *J Neurosci*. 2006;26:7281–7292.
39. Nilius B, Talavera K, Owsianik G, Prenen J, Droogmans G, Voets T. Gating of TRP channels: a voltage connection? *J Physiol*. 2005;567:35–44.
40. Dai L, Garg V, Sanguinetti MC. Activation of Slo2.1 channels by niflumic acid. *J Gen Physiol*. 2010;135:275–295.
41. Yang FC, Tan T, Huang T, et al. Genetic control of the segregation of pain-related sensory neurons innervating the cutaneous versus deep tissues. *Cell Rep*. 2013;5:1353–1364.
42. Olesen J, Diener HC, Husstedt IW, et al. Calcitonin gene-related peptide receptor antagonist BIBN 4096 BS for the acute treatment of migraine. *N Engl J Med*. 2004;350:1104–1110.
43. Engel MA, Khalil M, Siklosi N, et al. Opposite effects of substance P and calcitonin gene-related peptide in oxazolone colitis. *Dig Liver Dis*. 2012;44:24–29.
44. Verge VM, Richardson PM, Wiesenfeld-Hallin Z, Hökfelt T. Differential influence of nerve growth factor on neuropeptide expression in vivo: a novel role in peptide suppression in adult sensory neurons. *J Neurosci*. 1995;15:2081–2096.
45. Larsson J, Ekblom A, Henriksson K, Lundeberg T, Theodorsson E. Concentration of substance P, neurokinin A, calcitonin gene-related peptide, neuropeptide Y and vasoactive intestinal polypeptide in synovial fluid from knee joints in patients suffering from rheumatoid arthritis. *Scand J Rheumatol*. 1991;20:326–335.
46. Mikami N, Watanabe K, Hashimoto N, et al. Calcitonin gene-related peptide enhances experimental autoimmune encephalomyelitis by promoting Th17-cell functions. *Int Immunol*. 2012;24:681–691.
47. Holzer P. Neurogenic vasodilatation and plasma leakage in the skin. *Gen Pharmacol*. 1998;30:5–11.
48. Egea SC, Dickerson IM. Direct interactions between calcitonin-like receptor (CLR) and CGRP-receptor component protein (RCP) regulate CGRP receptor signaling. *Endocrinology*. 2012;153:1850–1860.
49. Sun H, Dodick DW, Silberstein S, et al. Safety and efficacy of AMG 334 for prevention of episodic migraine: a randomized, double-blind, placebo-controlled, phase 2 trial. *Lancet Neurol*. 2016;15:382–390.
50. Sulem P, Helgason H, Oddson A, et al. Identification of a large set of rare complete human knockouts. *Nature Genetics*. 2015;47:448–452.